June, 2007

Surface Friction Guiding for Reduced High-Frequency Lateral Vibration of Moving Media

V. Kartik
Jonathan A. Wickert, *Carnegie Mellon University*

Surface Friction Guiding for Reduced High-Frequency Lateral Vibration of Moving Media

V. Kartik
Mem. ASME
IBM Research Laboratory,
CH-8803 Rueschlikon, Zurich, Switzerland

J. A. Wickert[1]
Fellow ASME
Department of Mechanical Engineering,
Carnegie Mellon University,
Pittsburgh, PA 15213
e-mail: wickert@cmu.edu

The free and forced vibration of a moving medium is examined in an application where distributed friction guiding is used to control lateral position passively. Subambient pressure features formed in the guides intentionally modify the naturally occurring self-pressurized air bearing and increase the contact force between the medium and the guide's surface. These features increase friction to a level beyond that achievable based on the nominal wrap pressure. The moving medium is modeled as a beam that is transported over frictional regions and subjected to prescribed boundary disturbances arising from runout of a supply or take-up roll. For axial transport at a speed that is high compared to the velocity of lateral vibration, Coulomb friction between the guides and the moving medium can be well approximated by a derived expression for equivalent viscous damping. The equation of motion is developed for the cases of a single cylindrical guide and of a multiplicity of guides having arbitrary placement. The level of equivalent damping for each mode decreases with transport speed, and critical speeds exist where each vibration mode transitions between the overdamped and underdamped regimes. Parameter studies in the contact pressure, transport speed, and guide geometry identify preferred design configurations for maximizing dissipation in particular modes and for attenuating high-frequency response. [DOI: 10.1115/1.2732354]

1 Introduction

In magnetic tape libraries used for high-density data storage, lateral in-plane vibration of the tape undesirably misaligns the data tracks relative to the read/write head. Lateral motion arises from excitation sources, including the runout of supply and take-up packs, and roller guides, and from impacts between the tape and the flanges on packs and guides. The read/write head structure is conventionally mounted on a servotracking mechanism that can follow the tape's vibration up to a certain cutoff frequency, but higher-frequency vibration is problematic. The head is preferably positioned on a data track within 5% of the track's width to write data, and within 10% to read. To achieve reliable read/write operations in the presence of even submicron lateral vibration, each bit cell in a data track must be many times wider than its length in the transport direction. Reducing the bit cell's aspect ratio by reducing lateral tape vibration provides one of the greatest opportunities for further increases in storage density.

Conventional guides apply constraint forces to the tape's narrow edge, but even at modest levels, those forces can lead to excessive wear and heating of the tape. The methodology of friction guiding eliminates edge contact in some portions of the path by distributing lateral forces over the substantially wider face of the tape. Flangeless grooved rollers and nonrotating cylindrical posts are examples of guides that use friction to constrain lateral motion of magnetic tape and of other weblike materials in industrial manufacturing applications.

Surface friction guiding is effective for reducing high-frequency lateral vibration, and for avoiding edge wear, but the method has traditionally been limited by insufficient contact pressure between the guide and the medium. The contact pressure depends primarily on the winding tension T, the guide's radius R, and the medium's width b. A "foil bearing" forms when air is entrained between the moving medium and the guide, and that thin film of air lubricates relative sliding motion between the adjacent surfaces. The analysis of coupled moving media and foil-bearing systems involves the simultaneous solution of the equations governing the medium's elastic deformation and the air bearing's pressure. One-dimensional models [1,2] treat the foil bearing as being infinitely wide and are useful to calculate displacement and pressure along the bearing's centerline. In the steady state, the air pressure rises from the ambient atmospheric value at the bearing's inlet to the central value of approximately T/Rb. In the exit region, where a flow constriction develops, the pressure sharply rises and dips below ambient. Finite-width models additionally incorporate the effect of airflow out of the bearing's sides. Solution procedures include direct simulation of the equilibrium equations [3,4], inexact Newton iteration for faster convergence, and adaptive mesh allocation to reduce the number of nodal points needed in discretization [5]. The influence of surface curvature has also been incorporated in a dynamic model of the foil bearing [6].

To establish direct frictional contact, the air bearing can be vented intentionally by incorporating slots and channels on the surface of the guide [7]. One embodiment of a friction guide is shown in Fig. 1, where the lateral slot and pressure relief channel are intended to vent the air bearing that would otherwise form. The surface's geometry can include other subambient features that increase the contact pressure well beyond T/Rb as generated by the wrap geometry alone. Alternatively, increased contact pressure can be achieved with porous guides that develop suction through an external pump. In either manner, higher friction forces develop than would otherwise be achievable by, for instance, engineering surfaces having a higher coefficient of friction. In turn, the frictional forces attenuate high-frequency lateral vibration of the tape.

Ono [8] analyzed the mechanics of a moving string where lateral position was controlled through friction with a cylindrical guide having constant radius. Coulomb friction between the guide and the string was approximated by viscous damping when the velocity of vibration was much smaller than the (orthogonal)

[1]Corresponding author.

Contributed by the Technical Committee on Vibration and Sound of ASME for publication in the JOURNAL OF VIBRATION AND ACOUSTICS. Manuscript received May 3, 2006; final manuscript received October 25, 2006. Associate Editor: I. Y. (Steve) Shen. Paper presented at the 2006 ASME International Mechanical Engineering Congress (IMECE2006), November 5–10, 2006, Chicago, IL.

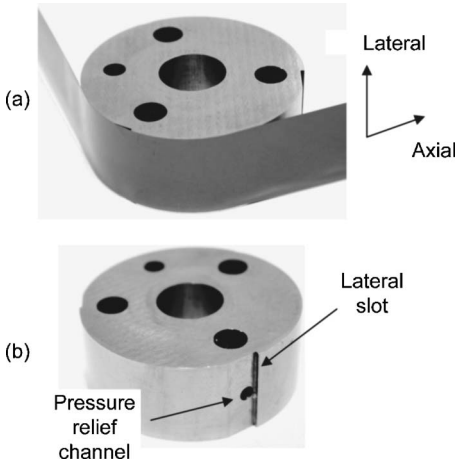

Fig. 1 (*a*) Magnetic tape is transported over a cylindrical surface friction guide that incorporates a subambient pressure feature. (*b*) The pressure relief channel vents the self-generated air bearing.

transport velocity. Yang [9] analyzed the dynamics of steady motion for threads moving over rotating rollers of arbitrary axisymmetric shape. A closed-form expression for response with a circular roller was compared to results for tapered and parabolic rollers. A rotating string in contact with point guides [10] has been taken as a model for the dynamics of more complex rotating and guided systems. The sensitivity of the natural frequencies with respect to the guide's stiffness and the rotation speed was examined, and the critical rotation speed was shown to be independent of stiffness. The vibration of beams in the presence of friction was analyzed in the context of systems where viscous damping had "stationary" and "moving" components [11]. The nature of the vibration response varied significantly even for seemingly small changes in the two damping coefficients. Also with a view toward dissipation sources, Garziera and Amabili [12] examined the effect of winding mechanics and the take-up roll's boundary condition on the damping of lateral vibration. Other related investigations have treated the linear response of a traveling string guided by an elastic support with dry friction [13], the stability of an axially accelerating string subjected to pointwise frictional forces [14], and free vibration of a traveling string that couples with a stationary spring-mass-damper subsystem [15].

The objective of this paper is to evaluate the free and steady-state forced response of a moving medium in the presence of friction that is provided by distributed guides having subambient pressure features. The moving medium is treated as a flexible beam that translates over spatially distributed guides. Vibration is excited by prescribed motion applied at the end points as caused by runout of the supply and take-up rolls. For transport at a high speed relative to the velocity associated with vibration, the Coulomb friction between the guides and moving medium is shown to be well approximated by equivalent viscous dissipation. The equations describing the beam's dynamics are developed for motion across a single cylindrical guide and are then extended to multiple guides of arbitrary placement and friction characteristics. The eigenvalue structure exhibits critical speeds where each mode transitions between the overdamped and underdamped regimes. The forced response of the medium is obtained for harmonic boundary excitation, and the efficacy of friction guides in attenuating high-frequency vibration is examined. Parameter studies identify opportunities to optimize the design of such surface friction guides.

2 Measurement

Figure 2 depicts an experimental magnetic tape transport system (Advanced Research Corporation) having three flanged post

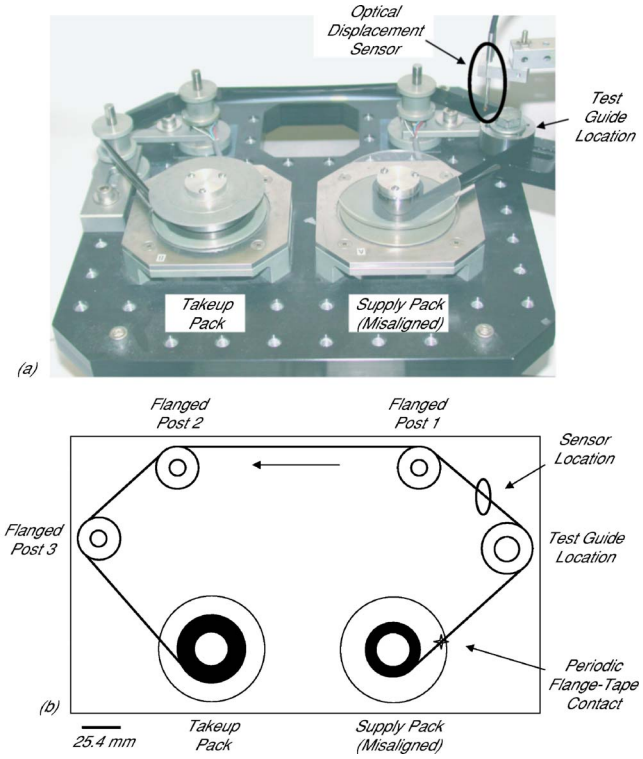

Fig. 2 (*a*) Tape transport test stand for friction guiding measurements, (*b*) the path comprises three flanged posts and one test guide

guides and one test guide that can either be a smooth cylindrical guide, which forms a self-pressurized air bearing, or a surface friction guide of the type shown in Fig. 1. The supply pack was adjacent to the test guide, and the pack's flange was intentionally misaligned to graze the tape during each rotation of the pack as the tape was unwound. An optical displacement sensor (MTI Instruments) was used to measure the lateral displacement of the tape at a position slightly downstream of the test guide's location in Fig. 2(*b*). The three flanged posts between the sensor and the take-up pack reduced the component of displacement occurring at the sensor's location that arose from the take-up pack's smaller runout.

Measurements were performed for two different test guides. In the baseline case, the tape passed over a cylindrical guide of width and radius identical to the one shown in Fig. 1 but without the subambient pressure features. The smooth surface enabled an air bearing to develop between the moving tape and the guide's surface. In the second case, the friction guide of Fig. 1 was oriented such that the subambient pressure slot engaged the tape's wrap with direct frictional contact. In both cases, the 9 μm thick and 12.65 mm wide tape was transported between the supply and take-up packs at 4 m/s and under a tension of 1 N. Lateral vibration was measured at a sampling frequency of 5 kHz. Figure 3 depicts typical displacement records for the two cases. The addition of friction damping reduced the peak-to-peak vibration amplitude from 45 μm to 20 μm. Most notably, the amplitude reduction was achieved without contact between the tape's relatively fragile edge and the guide. Figure 4 depicts the corresponding frequency spectra. The amplitude of the 100 Hz component that arose from rotation of the supply pack decreased from nearly 20 μm to 5 μm through friction guiding. The near total reduction in Fig. 4(*b*) of the higher harmonic content is particularly advantageous to the extent that those components are poorly compensated by the read/write head's tracking servomechanism.

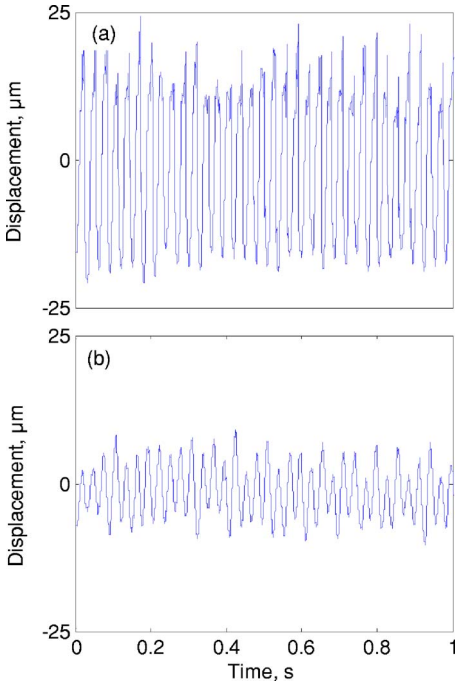

Fig. 3 Measured lateral vibration at the test guide's location (*a*) with a conventional air bearing guide and (*b*) with a friction guide that incorporates subambient pressure features

3 Friction Guiding Vibration Model

Figure 5 shows, in schematic form, a transport system for a tape, web, or any other flexible moving medium that has two friction guides located between its end supports. The medium is modeled as an Euler-Bernoulli beam that convects at the constant speed v over guides of radii $R^{(1)}$ and $R^{(2)}$, respectively. The guided segments are the regions $[x_0^{(1)},x_e^{(1)}]$ and $[x_0^{(2)},x_e^{(2)}]$, and they are

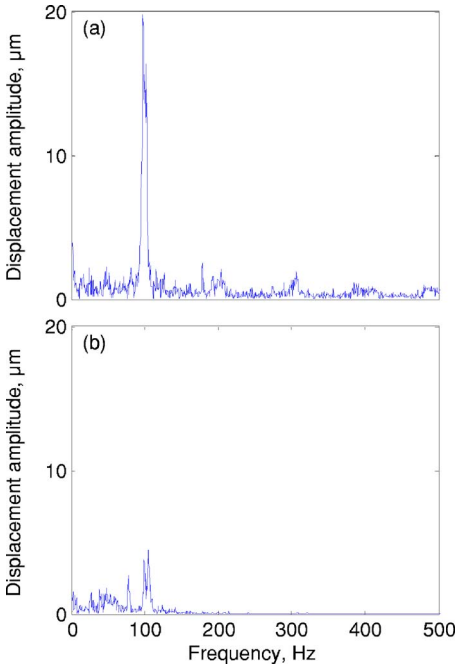

Fig. 4 Measured spectra for lateral vibration at the test guide's location (*a*) with a conventional air bearing guide and (*b*) with a friction guide that incorporates subambient pressure features

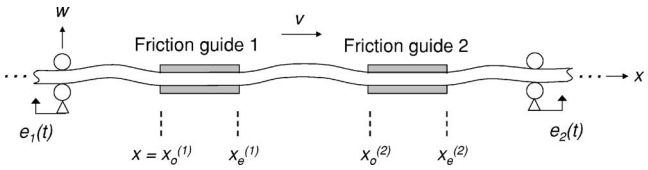

Fig. 5 Schematic diagram of a beam translating over two distributed contact friction guides and excited by prescribed displacements at its boundaries

intended to constrain and control the beam's lateral vibration w in the central portion $(x_e^{(1)},x_0^{(2)})$. The supports are located at $x=0$ and $x=L$, and have prescribed motions $e_1(t)$ and $e_2(t)$ that arise from runout of the supply and take-up rolls. The beam has width b, cross-sectional area A, mass density ρ, and flexural rigidity EI. In Fig. 6, a segment of the beam is isolated in the contact region between points S_1 and S_2 on its neutral axis. In many tape or web-handling applications, the flexural rigidity in the transverse direction is negligible when compared to that in the lateral direction, and therefore the tension gradient across the beam's thickness, which arises from the guide's curvature, is neglected here. The tension, however, does increase from $T_0^{(i)}$ to $T_e^{(i)}$ across $[x_0^{(i)},x_e^{(i)}]$ owing to friction. The tension is constant in the free spans $(0,x_0^{(1)})$, $(x_e^{(1)},x_0^{(2)})$, and $(x_e^{(2)},L)$, but it attains a different value in each.

Over the span of any particular guide i out of the total NG guides, a reaction of magnitude $N^{(i)}$ per unit of length acts on the beam and is directed outward from, and normal to, the guide's surface at P. The friction force $\mathbf{F}^{(i)}$ per unit of length acts in the plane of the guide's surface, and it is modeled here in the classical Coulomb form. By applying the analysis developed in [8] for a string in contact with a cylindrical guide, friction develops in response to two velocity components: the beam's transport speed v along its neutral axis and the lateral velocity associated with w. The lateral component of $\mathbf{F}^{(i)}$ changes direction in response to vibration, while the axial component opposes steady transport and does not reverse direction. The friction force per unit of length becomes

$$\mathbf{F}^{(i)} = -N^{(i)} \begin{bmatrix} \mu_x^{(i)} & 0 \\ 0 & \mu_z^{(i)} \end{bmatrix} \frac{d\mathbf{r}/dt}{|d\mathbf{r}/dt|} \tag{1}$$

where t denotes time, $\mathbf{r}$ is the position vector of P relative to the guide, and $|\cdot|$ denotes vector magnitude. Here, $\mu_x^{(i)}$ and $\mu_z^{(i)}$ are the coefficients of friction in the x and z directions. The quantity

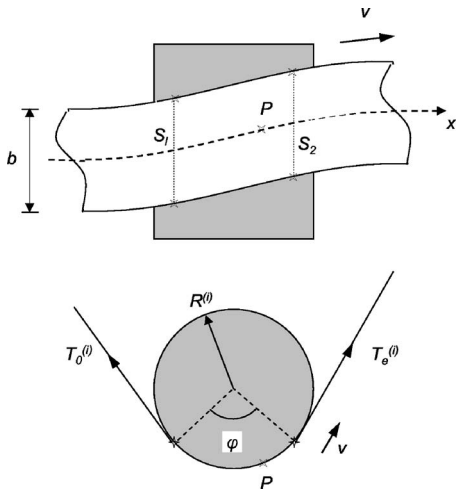

Fig. 6 Detail of the contact region on a friction guide

$(d\mathbf{r}/dt)/|d\mathbf{r}/dt|$ sets the direction of the friction force to oppose the strip's instantaneous velocity. In applying Eq. (1) to the motivating technology, the transport speed for computer storage applications is on the order of several meters per second, substantially exceeding the peak vibration velocity in the lateral direction, which is only on the order of centimeters per second. With the approximation $|d\mathbf{r}/dt| \approx v$, Eq. (1) becomes

$$\mathbf{F}^{(i)} = -\begin{bmatrix} \mu_x^{(i)} & 0 \\ 0 & \mu_z^{(i)} \end{bmatrix} \left(\frac{N^{(i)}}{v}\right) \frac{d\mathbf{r}}{dt} \tag{2}$$

and the dissipation in this particular situation can be well approximated by an equivalent viscous damping model (Appendix A).

The beam's tension across guide i increases exponentially according to

$$T^{(i)}(x) = [T_0^{(i)} + p^{(i)}R^{(i)}b] \exp\left\{\frac{\mu_x^{(i)}}{R^{(i)}}[x - x_0^{(i)}]\right\} - p^{(i)}R^{(i)}b \tag{3}$$

for $x \in [x_0^{(i)}, x_e^{(i)}]$, where $1 \le i \le NG$, $T_0^{(i)}$ is the tension at $x_0^{(i)}$, and $p^{(i)}$ is the subambient pressure generated over the guide. The normal reaction becomes

$$N^{(i)}(x) = \frac{T^{(i)}(x)}{R^{(i)}} + p^{(i)}b \tag{4}$$

The equation of motion governing the beam's lateral vibration over $(0,L)$ is

$$\rho A(w_{,tt} + 2vw_{,xt} + v^2 w_{,xx}) - [T(x)w_{,x}]_{,x} + (EIw_{,xx})_{,xx} = -\sum_{i=1}^{NG} \frac{\mu_z^{(i)}}{v}\left[\frac{T^{(i)}(x)}{R^{(i)}} + p^{(i)}b\right](w_{,t} + vw_{,x})W^{(i)}(x) \tag{5}$$

where $W^{(i)}$ is a windowing function having unit value over the ith guide and vanishing elsewhere. Equation (5) has terms corresponding to the local, Coriolis, and centripetal acceleration components, the spatially varying tension, and the friction that develops in response to the total velocity $(w_{,t}+vw_{,x})$ as measured by a stationary observer. With the dimensionless variables

$$x^* = \frac{x}{L}, \quad w^* = \frac{w}{L}, \quad b^* = \frac{b}{L}, \quad R^{*(i)} = \frac{R^{(i)}}{L} \tag{6}$$

$$t^* = t\sqrt{\frac{EI}{\rho AL^4}}, \quad v^* = v\sqrt{\frac{\rho AL^2}{EI}}, \quad T^{(i)*} = \frac{T^{(i)}L^2}{EI}, \quad p^{(i)*} = \frac{p^{(i)}L^4}{EI} \tag{7}$$

Equation (5) is recast as

$$w^*_{,t^*t^*} + 2v^* w^*_{,x^*t^*} + v^{*2} w^*_{,x^*x^*} - (T^*(x^*)w^*_{,x^*})_{,x^*} + w^*_{,x^*x^*x^*x^*} = -\sum_{i=1}^{NG} \frac{\mu_z^{(i)}}{v^*}\left[\frac{T^*(x^*)}{R^{*(i)}} + p^{*(i)}b^*\right](w^*_{,t^*} + v^* w^*_{,x^*})W^{(i)}(x^*) \tag{8}$$

The beam's forced response is determined for the prescribed motions $e_1^* = e_1/L$ and $e_2^* = e_2/L$ at its end points and subject to the conditions $w^*_{,x^*x^*}(0,t^*) = w^*_{,x^*x^*}(1,t^*) = 0$. The time-varying boundary conditions are rendered homogeneous through the shift of coordinates

$$w^* = u^* + (1 - x^*)e_1^* + x^* e_2^* \tag{9}$$

in terms of the new displacement field u^*, which satisfies $u^* = u^*_{,x^*x^*} = 0$. The working form of the equation of motion becomes

$$\begin{aligned} &u^*_{,t^*t^*} + 2v^* u^*_{,x^*t^*} + v^{*2} u^*_{,x^*x^*} - (T^* u^*_{,x^*})_{,x^*} + u^*_{,x^*x^*x^*x^*} + \sum_{i=1}^{NG} \frac{\mu_z^{(i)}}{v^*}\left[\frac{T^*(x^*)}{R^{*(i)}} + p^{*(i)}b^*\right](u^*_{,t^*} + v^* u^*_{,x^*})W^{(i)}(x^*) \\ &= -(1 - x^*)e_1^{*\prime\prime} + \left\{2v^* - \sum_{i=1}^{NG} \frac{\mu_z^{(i)}}{v^*}\left[\frac{T^*(x^*)}{R^{*(i)}} + p^{*(i)}b^*\right](1 - x^*)W^{(i)}(x^*)\right\} e_1^{*\prime} - \left\{[T^*(x^*)_{,x^*}]_{,x^*} + \sum_{i=1}^{NG} \mu_z^{(i)}\left[\frac{T^*(x^*)}{R^{*(i)}} + p^{*(i)}b^*\right]W^{(i)}(x^*)\right\} e_1^* \\ &\quad - x^* e_2^{*\prime\prime} - \left\{2v^* - \sum_{i=1}^{NG} \frac{\mu_z^{(i)}}{v^*}\left[\frac{T^*(x^*)}{R^{*(i)}} + p^{*(i)}b^*\right]x^* W^{(i)}(x^*)\right\} e_2^{*\prime} + \left\{[T^*(x^*)_{,x^*}]_{,x^*} + \sum_{i=1}^{NG} \mu_z^{(i)}\left[\frac{T^*(x^*)}{R^{*(i)}} + p^{*(i)}b^*\right]W^{(i)}(x^*)\right\} e_2^* \end{aligned} \tag{10}$$

where $(\cdot)' = d/dt^*$ and is subject to $u^*(0,t^*) = u^*(1,t^*) = u^*_{,x^*x^*}(0,t^*) = u^*_{,x^*x^*}(1,t^*) = 0$.

Previous work in the area of moving media vibration has addressed the response to general forms of excitation by using modal analysis and Green's function methods [16–19]. A variety of expansion functions can be used in the discretization of Eq. (10). For instance, in the stability analysis of a traveling beam in contact with an elastic point guide [20], the complex normal modes of an unguided beam were used to obtain the free and forced response solutions. In [21], discretization methods and their accuracy and convergence characteristics were discussed for a variety of expansion function choices. A basis comprising modes of a translating beam did not exhibit better convergence than one comprising modes of a nontranslating beam. Here, the orthonormal basis $X_n = \sqrt{2}\sin(n\pi x^*)$, for $n = 1,2,\ldots,NU$, constitutes solutions to the proximate problem for vibration of a nontranslating beam without friction, and it satisfies the essential boundary conditions of Eq. (10). With the separable series solution $u^* = \sum_{n=1}^{NU} X_n(x^*)\eta_n(t^*)$, the discretized form of the equation of motion becomes

$$\underline{M}\,\underline{\eta}'' + (\underline{C} + \underline{G})\,\underline{\eta}' + (\underline{K}_c + \underline{K}_{nc})\,\underline{\eta} = \underline{f} \tag{11}$$

which includes the symmetric and speed-dependent damping matrix $\underline{C}$ associated with friction in Eq. (2) and the skew-symmetric gyroscopic matrix $\underline{G}$ associated with Coriolis acceleration. The stiffness matrix comprises the conservative component $\underline{K}_c$ representing the beam's flexural rigidity and tension, and the nonconservative component $\underline{K}_{nc}$ that arises from the dissipation component that is proportional to $vw_{,x}$. Elements of these matrices are listed in Appendix B. The solution of the complex eigenvalue problem yields the mode shapes and natural frequencies. The eigenfunctions are complex $(\psi_n = \psi_n^R + i\psi_n^I, n = 1,2,\ldots)$, and the

real parts of the eigenvalues λ_n^* determine the level of modal damping.

4 Natural Frequency and Mode Structure

4.1 Analogous Guided String Model. The structure of the eigenvalue loci and the onset of critical damping for Eq. (10) can be interpreted in the context of a simpler, but analogous, model for which a closed-form solution is available. When a string is transported between end supports and is in contact with a frictional surface of the form (2) over its entire length, an eigenvalue structure results that is similar to that for the beam. By only neglecting the tension gradient $T_{,x}$ here the nondimensional equation of motion for this alternative system is

$$u^*_{,t^*t^*} + 2v^* u^*_{,x^*t^*} + (v^{*2} - 1)u^*_{,x^*x^*} + \left(\frac{2\mu_z\beta^*}{v^*}\right)(u^*_{,t} + v^* u^*_{,x}) = 0 \tag{12}$$

where $u^* = u/L$, $v^* = v/\sqrt{T/\rho A}$, and $\beta^* = (L/2R)(1 + pbR/T)$ is the nondimensional contact force per unit of length. With the solution form $u^* = \exp(\lambda^* t^* + \gamma^* x^*)$, Eq. (12) yields the dispersion relation

$$(v^{*2} - 1)\gamma^{*2} + 2(v^*\lambda^* + \mu_z\beta^*)\gamma^* + \lambda^{*2} + \left(\frac{2\mu_z\beta^*}{v^*}\right)\lambda^* = 0 \tag{13}$$

between eigenvalues λ^* and wave numbers γ^*, with roots

$$\gamma^{*(1,2)} = \frac{1}{1 - v^{*2}}\left\{(v^*\lambda^* + \mu_z\beta^*) \pm \left[\lambda^{*2} + \left(\frac{2\mu_z\beta^*}{v^*}\right)\lambda^* + (\mu_z\beta^*)^2\right]^{1/2}\right\} \tag{14}$$

Applying the end conditions $u^*(0,t) = u^*(1,t) = 0$, the characteristic equation for the string's vibration yields the nth eigenvalue pair

$$\lambda_n^{*(1,2)} = -\left(\frac{\mu_z\beta^*}{v^*}\right) \pm i\left\{\left[(n\pi)^2(1 - v^{*2}) - \left(\frac{\mu_z\beta^*}{v^*}\right)^2\right](1 - v^{*2})\right\}^{1/2} \tag{15}$$

In the absence of friction, the eigenvalues reduce to $\lambda_n^{*(1,2)} = \pm i(n\pi)(1 - v^{*2})$, which is the expected classical solution for a traveling string. For $v^* < 1$, the natural frequencies decrease monotonically with friction until each mode becomes critically damped at $\beta^*_{cr} = 2(n\pi v^*)^2\sqrt{1 - v^{*2}}/\mu_z$. A notable characteristic of the eigenvalue structure in Eq. (15) is the independence of $\mathrm{Re}(\lambda_n^*)$ from the mode number n. The magnitude $|\mathrm{Re}(\lambda_n^*)|$ for each eigenvalue pair increases with friction and contact pressure, but it decreases asymptotically with v^*. Similar characteristics are present in the solutions to Eq. (10), as discussed next.

4.2 Tensioned Beam Eigenvalues and Mode Shapes. The model (10) is applied to the two guide system[2] in Fig. 5. The subambient pressure characteristic of the guides is defined by coefficient α that represents the fraction of atmospheric pressure generated beyond the nominal wrap pressure. In the absence of friction, the eigenvalues of the beam are strictly imaginary and nonzero. As the transport speed increases, the natural frequencies progressively decrease until the first critical speed is reached, at which point the fundamental frequency vanishes. The addition of friction, which varies inversely with speed in Eqs. (2) and (10), has a stabilizing effect. In Fig. 7, the evolution with increasing

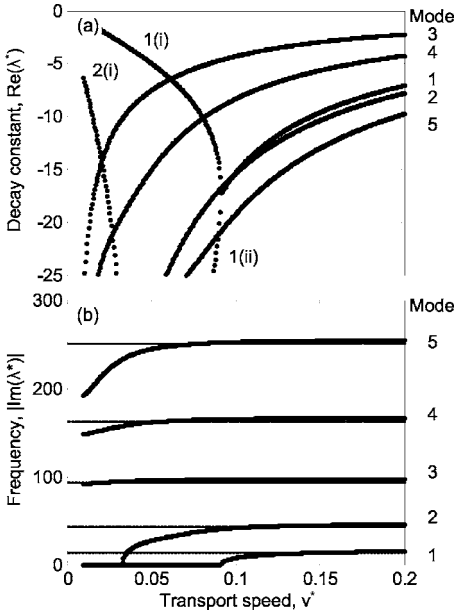

Fig. 7 (*a*) Real and (*b*) imaginary eigenvalue component loci with increasing transport speed; $\mu_z = 0.1$ and $\alpha = 0.2$. The first two modes have branches labeled (i) and (ii) that bifurcate at critical speeds for overdamping. The frequency loci for an unguided beam are shown by the lighter line.

transport speed of the eigenvalues is depicted for $\mu_z = 0.1$ and $\alpha = 0.2$. For the (low-) speed range shown in Fig. 7, each real eigenvalue component is negative. The lowest speed shown in Fig. 7 ($v^* = 0.01$) is still an order of magnitude greater than the lowest speed at which the equivalent viscous approximation (2) is valid for vibration amplitudes that are typical of the motivating application. At that speed, the eigenvalues corresponding to the third and higher vibration modes are complex. For $v^* \leq 0.04$, the lowest two modes are overdamped, with each locus being bifurcated. Both branches of the first locus, denoted 1(i) and 1(ii), as well as one branch of the second locus are discernible over the range of ordinate values shown in Fig. 7. As the level of friction damping decreases with v^*, the two real companion branches converge until the mode becomes critically damped, and subsequently at higher speeds, underdamped. In this illustrative case, critical damping occurs at $v^* = 0.09$ for the first mode and at $v^* = 0.04$ for the second mode. For $v^* > 0.09$, all modes are underdamped. After the real eigenvalue branches for any mode have coalesced, further increases in v^* drive the decay constants $|\mathrm{Re}(\lambda^*)|$ to decrease monotonically.

In Fig. 8(*a*), the evolution of eigenvalues with v^* is shown for the beam with friction acting over the entire span $x \in (0,1)$, instead of over the two distributed guiding regions. This eigenvalue structure follows the qualitative behavior exhibited in Eq. (15) for the string model, and it is also similar to that of Fig. 7, where overdamped modes become underdamped at certain speeds. Analogous to Eq. (15), the $\mathrm{Re}(\lambda_n^*)$ pairs for any overdamped mode converge in Fig. 8(*a*) to a common asymptotic locus. However, with the transition to a partial frictional foundation over $[x_0^{*(1)}, x_e^{*(2)}]$ as in Fig. 8(*b*), the dissipation for individual modes develops with friction to different extents. Damping $\mathrm{Re}(\lambda^*)$ becomes dependent on the particular mode, and the $\mathrm{Re}(\lambda_n^*)$ loci are distinct. This behavior in Fig. 7 is therefore attributed to the particular placement of the guides rather than to the distributed friction mechanism itself. As the width of the guided span(s) narrows in Figs. 8(*a*)–8(*c*), the first mode transitions from the overdamped to the underdamped regimes at lower transport speeds.

Figure 9 depicts evolution of the eigenvalues with respect to α

[2]Unless noted otherwise, the model parameters are as follows: axial friction coefficient, $\mu_x = 0.1$; lateral friction coefficient, $\mu_z = 0.1$; tension at $x^* = 0$, $T_0^* = 8.65$; transport speed, $v^* = 0.15$; central position of guide 1, $x^* = 0.3$; central position of guide 2, $x^* = 0.7$; guide wrap angles, $\phi^{(i)} = \pi/4$; and guide radii, $R_g^{*(i)} = 0.159$.

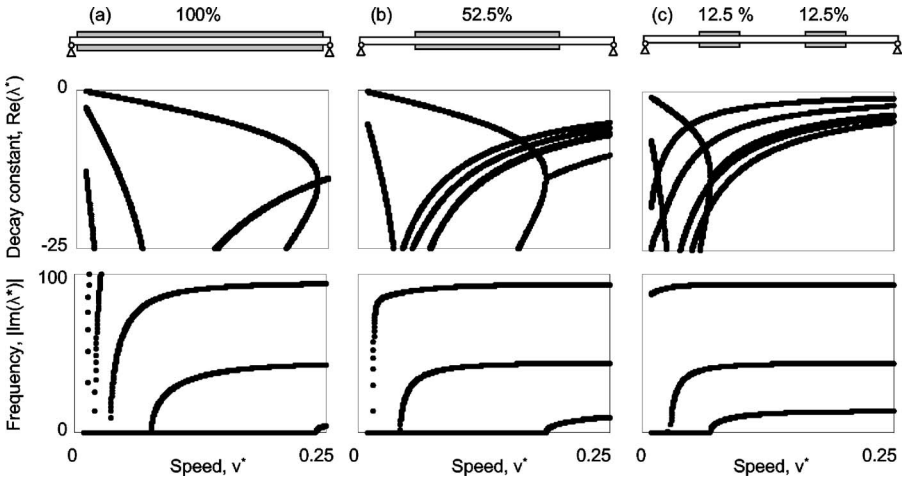

Fig. 8 Evolution of the eigenvalue loci with transport speed for three choices of guide placement: (*a*) full friction guiding over $x^* \in (0,1)$, (*b*) partial guiding over $x^* \in [x_0^{*(1)}, x_e^{*(2)}]$, and (*c*) two narrow guides with placement as in Fig. 5

for the dual guide system of Fig. 5. The contact pressure contributes to the beam's stiffness in several respects; in Eq. (10), dissipation introduces the nonconservative stiffness component $v^* w^*_{,x^*}$, and the beam's tension gradient increases stiffness. For the range of pressure coefficients depicted in Fig. 9, the first mode becomes increasingly damped as α grows, and the fundamental natural frequency vanishes near $\alpha=0.95$ at the critical damping condition. Over the same range of α, the third and higher frequencies rise in response to the tension gradient, the stiffening effect of which outweighs the frequency reduction associated with greater damping. In accordance with Eq. (15) for the analogous string model, the magnitude $|\mathrm{Re}(\lambda_n^*)|$ of the decay constant for each mode increases nearly linearly through $\alpha \leq 0.5$, although the loci are distinct here because of the placement of multiple guides.

Figure 10 depicts the first five mode shapes of the beam in Fig. 5 for $\alpha=0.02$. The mode shapes are complex, owing to convection and friction. The beam's tension gradient, in part, produces asymmetry in the shapes. In the light of Eq. (3), the relative increase in tension between the ends of a guide i depends not only on the guide's radius, wrap angle, and α, but also on $T_0^{(i)}$. Therefore, even though the guides are identical, the relative tension increases across guide $i=1$ is greater than that across guide $i=2$. The tension increases 19% between the ends of the first guide, and over 17% across the second guide. From a design standpoint, the increased tension due to friction should not exceed an allowable limit for the web material, and the guide's characteristics should be selected to maximize damping while satisfying any constraint on peak tension.

4.3 Parameter Selection for Overdamping. In a particular application, the transport speed can be dictated by considerations,

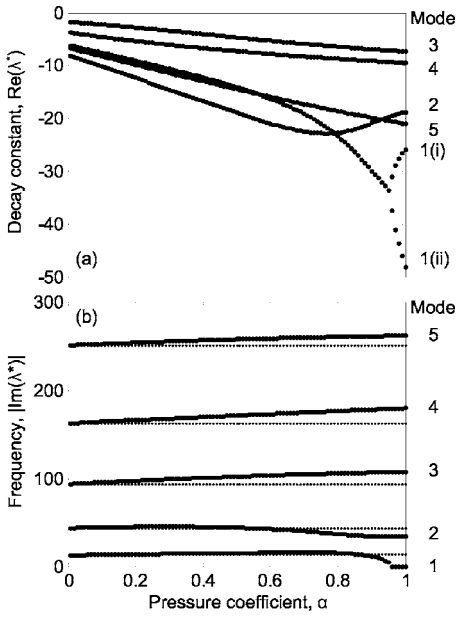

Fig. 9 (*a*) Real and (*b*) imaginary eigenvalue component loci with increasing subambient pressure, $\mu_z=0.1$ and $v^*=0.4$. The fundamental mode bifurcates into branches 1(i) and 1(ii) above the critical pressure coefficient for overdamping. The frequency loci for an unguided beam are shown by the lighter line.

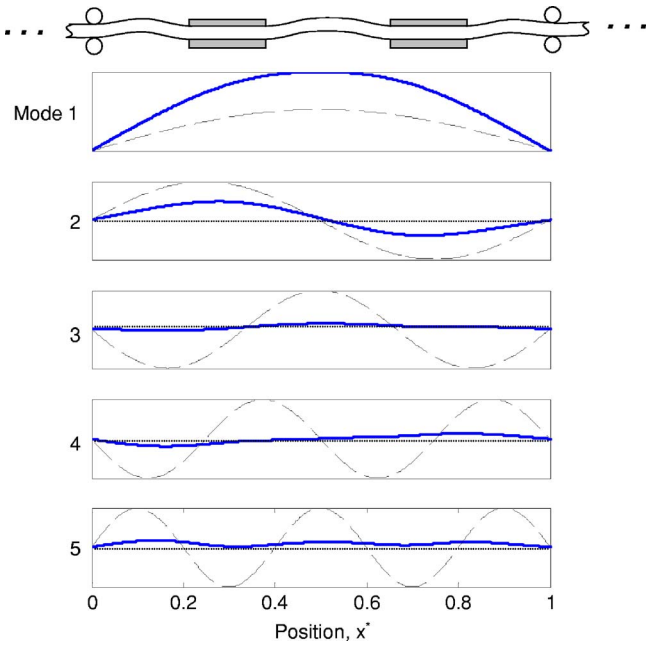

Fig. 10 First five mode shapes; $\alpha=0.02$. Real components are shown by the solid line, and imaginary components, the dashed line

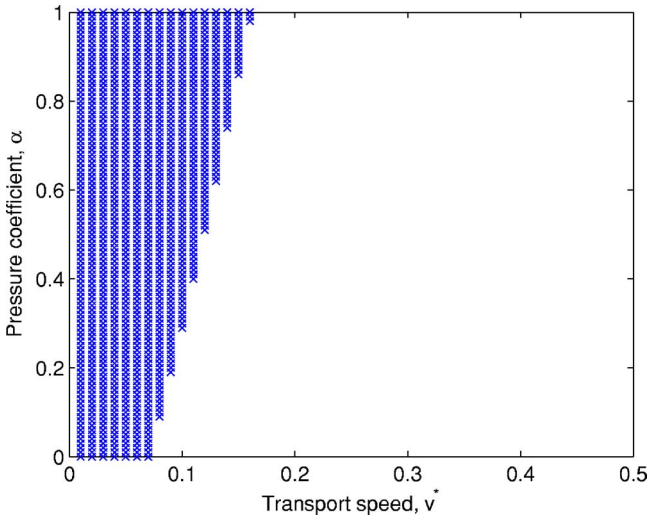

Fig. 11 Hatched region denotes $v^*-\alpha$ parameter combinations where the fundamental vibration mode is overdamped

such as transfer rates in data storage, printing rates in paper handling, or process requirements in sheet metal rolling. The guide's characteristics can be varied in such situations to increase friction damping, even to the point of overdamping certain modes. Figure 11 illustrates regimes in the $\alpha-v^*$ parameter plane where the fundamental mode is overdamped. At low α, the mode is overdamped only at the lowest speeds, and with $\alpha=0$, $v^*<0.08$ for overdamping. As the pressure coefficient is increased, however, the fundamental mode remains overdamped at higher speeds, even with the same value of the friction coefficient. In Fig. 12, the parameter region where the fundamental mode is overdamped is shown as a function of v^* and the wrap angle in Fig. 6. By increasing ϕ, greater friction is applied to the beam, and the fundamental mode remains overdamped across a broader range of speed.

5 Forced Response and High-Frequency Attenuation

Run out of the supply and take-up rolls can be a significant excitation source of lateral vibration. The response to sinusoidal motion $e_1^*=W_1^*\sin(\Omega_1^* t^*)$ at the left-hand boundary, where $W_1^*=W_1/L$ and $\Omega_1^*=\Omega_1/\sqrt{EI/\rho AL^4}$ are the dimensionless excitation amplitude and frequency, is depicted in Fig. 13. The beam's deflection is shown over one cycle of excitation for the representative value $\Omega_1^*=20$. At $\alpha=0$, the displacement over the two guided spans is similar to that without any guiding (dashed line type in Fig. 13(*a*)), indicating that the standard wrap pressure alone generates only a small amount of contact pressure and damping. With $\alpha=0.2$ (Fig. 13(*b*)), damping is sufficient to reduce the beam's amplitude over the guided regions, and the peak-to-peak displacement amplitude at midspan is reduced by nearly 60%. For a given Ω^*, however, increasing α improves attenuation only up to a point beyond which the degree of attenuation plateaus. For example, with $\Omega_1^*=20$, the amplitude at $x^*=0.45$ (a location offset from the nodes of the anti-symmetric modes) falls rapidly as subambient pressure is increased from $\alpha=0$ to $\alpha=0.05$ and reaches a minimum of 33% of the baseline displacement at $\alpha=0$. For $\alpha>0.05$, there is no substantial further decrease in amplitude even though the peak tension continues to increase.

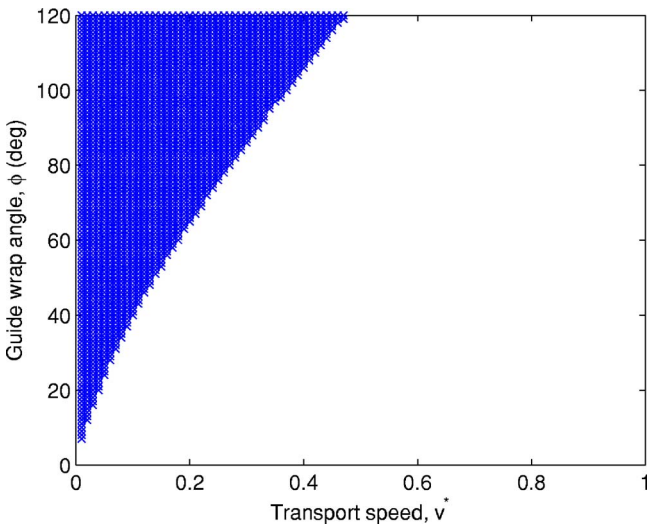

Fig. 12 Hatched region denotes $v^*-\phi$ parameter combinations where the fundamental vibration mode is overdamped

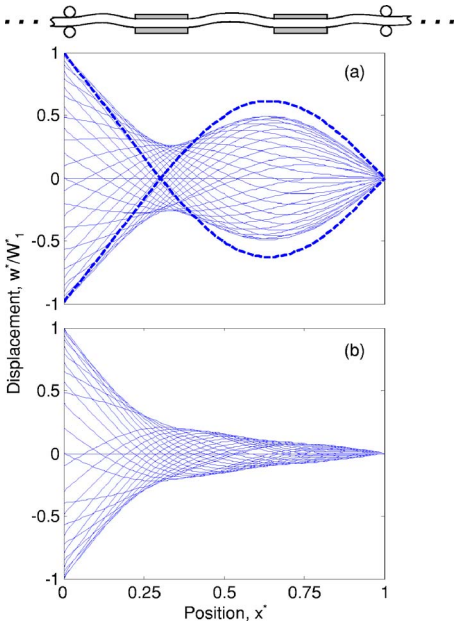

Fig. 13 Deflection envelope over one cycle of excitation with (*a*) ambient contact pressure ($\alpha=0$) and (*b*) subambient contact pressure ($\alpha=0.2$); $\Omega_1^*=20$. The dashed line in (*a*) denotes the envelope in the absence of friction.

A key feature of friction guiding for moving media is the ability to attenuate high-frequency vibration. Figure 14 depicts the beam's frequency response function at $x^*=0.45$ when it is subject to boundary motion e_1^*. With $\mu_z=0.1$ and the nominal belt wrap pressure ($\alpha=0$), only the first two modes are overdamped (Fig. 14(*b*)). However, with subambient pressure beyond the wrap pressure (Figs. 14(*c*) and 14(*d*)), all modes within the frequency range shown are favorably overdamped.

6 Summary

The free and forced lateral vibration of moving media in the presence of distributed friction guiding has been analyzed. Vibration is examined in the context of an application where subambient pressure features on the surface of the guide increase the contact force between the medium and the guide. With steady transport at a high speed relative to the lateral vibration velocity, Coulomb friction in this particular application can be well approximated by an equivalent viscous damping model. The magnitude of damping $|\mathrm{Re}(\lambda_n^*)|$ for each mode is speed dependent, and the eigenvalue structure exhibits critical speeds where each mode transitions between the overdamped and underdamped regimes. The tension gradient that arises along the length of the medium

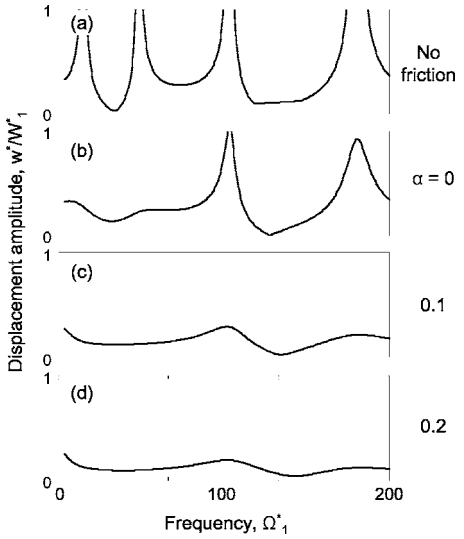

Fig. 14 Frequency response function at $x^*=0.45$ for different levels of friction guiding

distorts the mode shapes and limits the level of guide friction that can practically be imposed. Parameter studies are performed with respect to the pressure coefficient, transport speed, and guide placement in order to identify their contributions to dissipation. The subambient pressure guides are shown to be particularly effective for attenuating response at high frequencies.

Acknowledgment

This work was supported by Imation Corporation through the Multi-Terabyte Tape Storage program. The authors appreciate the assistance of Ted Schwarz, Rich Jewett, Chris Zwettler, Jim Anderson, Saeed Fahimi, and Doug Johnson with the work described herein.

Appendix A

The transition between the Coulomb and the viscous damping regimes in Eq. (2) is investigated here in the context of the analogous single-degree-of-freedom oscillator shown in Fig. 15. The mass m is attached by a spring of stiffness k to a frame traveling at constant speed v over a horizontal surface. Classical Coulomb friction is present between m and the surface. The mass is constrained to vibrate in the direction orthogonal to the frame's prescribed motion. In a manner similar to the beam of Fig. 5, the contacting surfaces do not stick and the directions of transport v and vibration w are orthogonal. The related problem involving self-excited vibration of an oscillator resting on a moving belt is discussed in [22], although in that case m vibrates in the same direction as the belt's velocity, and self-excitation of the oscillator's vibration occurs.

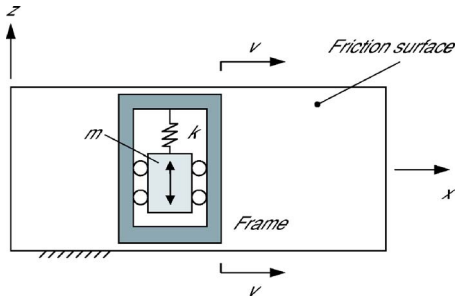

Fig. 15 Analogous single degree-of-freedom oscillator that undergoes lateral vibration in a frame that slides at speed v in the orthogonal direction over a surface with Coulomb friction. Force N acts orthogonal to the plane.

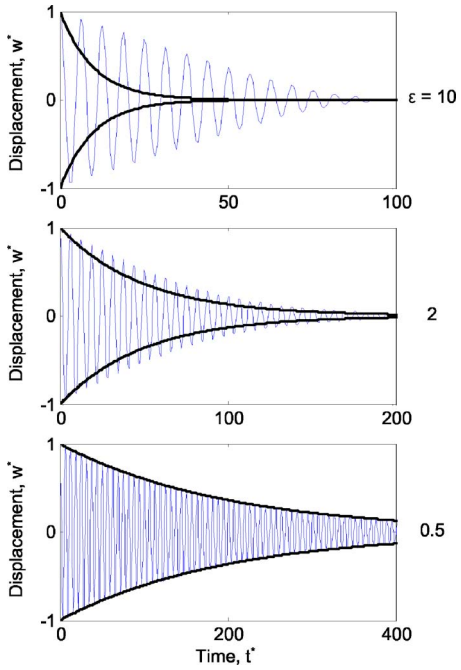

Fig. 16 Transient response of the analogous single-degree-of-freedom oscillator and frame system moving over a surface with Coulomb friction. The displacement envelope based on the approximation (A2) (dark line) is superposed on the numerical solution to Eq. (A1) (lighter line).

The friction force has components in the x and z directions; the former component opposes the frame's transport, and the latter opposes vibration w. In the absence of friction, the mass oscillates with maximum displacement w_0 and maximum velocity $w_0\sqrt{k/m}$. With friction, the amplitude of motion decays with time in a manner dependent on w_0 and v. With N denoting the magnitude of the normal reaction force between m and the surface, and μ being the friction coefficient, the oscillator's nondimensional equation of motion in the z direction is

$$w^{*\prime\prime} + \frac{\mu N^*}{\sqrt{v^{*}2 + w^{*\prime 2}}} w^{*\prime} + w^* = 0 \tag{A1}$$

where $(\cdot)^*$ denotes a nondimensional quantity. With the representative value $\mu=0.1$, Eq. (A1) can be simulated numerically for different ratios $\epsilon=(\sqrt{k/m})(w_0/v)$, and the results are shown in Fig. 16. For $\epsilon \ll 1$, $\sqrt{1+(w^{*\prime}/v^*)^2} \approx 1$, and the displacement decay envelope based on the equivalent viscous approximation

$$w^{*\prime\prime} + \left(\frac{\mu N^*}{v^*}\right) w^{*\prime} + w^* = 0 \tag{A2}$$

is shown superposed over the numerically determined displacement from Eq. (A1). For a low transport speed ($\epsilon=10$), the envelope of the mass's decaying motion is sensibly linear, consistent with the dominating Coulomb mechanism. As the transport speed increases relative to the maximum velocity of the mass's oscillation, the decay envelope more closely approximates the exponential character of the viscous damping approximation. Even for $\epsilon=0.5$, the actual displacement envelope, and the approximate viscous damping envelope, are indistinguishable in Fig. 16.

Appendix B

The elements of the matrices in Eq. (11) are ($\delta_{mn}=1$ if $m=n$, $\delta_{mn}=0$ otherwise):

$$M^{(m,n)} = \frac{1}{2}\delta_{mn} \tag{B1}$$

$$C^{(m,n)} = \frac{1}{v^*}\sum_{i=1}^{NG} \frac{\mu_z^{(i)}}{R^{*(i)}} T^*[x_0^{*(i)}] \int_{x_0^{*(i)}}^{x_e^{*(i)}} \exp\left\{ \frac{\mu_x^{(i)}[x^* - x_0^{*(i)}]}{R^{*(i)}} \right\} \times \sin(m\pi x^*) \sin(n\pi x^*) dx \tag{B2}$$

$$G^{(m,n)} = nv^* \left[\frac{1-(-1)^{m+n}}{m+n} - \frac{1-(-1)^{m-n}}{m-n} \right](1-\delta_{mn}) \tag{B3}$$

$$\begin{aligned} K_c^{(m,n)} = {} & \frac{(n\pi)^4}{2}\delta_{mn} - \frac{(n\pi v^*)^2}{2}\delta_{mn} + (n\pi)^2 \sum_{i=1}^{NG} T^*[x_0^{*(i)}] \\ & \times \int_{x_0^{*(i)}}^{x_e^{*(i)}} \exp\left(\frac{\mu_x^{(i)}(x^* - x_0^{*(i)})}{R^{*(i)}} \right) \sin(m\pi x^*) \sin(n\pi x^*) dx^* \\ & - (n\pi) \sum_{i=1}^{NG} \frac{\mu_z^{(i)}}{R^{*(i)}} T^*(x_0^{*(i)}) \\ & \times \int_{x_0^{*(i)}}^{x_e^{*(i)}} \exp\left(\frac{\mu_x^{(i)}(x^* - x_0^{*(i)})}{R^{*(i)}} \right) \sin(m\pi x^*) \cos(n\pi x^*) dx^* \\ & + (n\pi)^2 T^*(0) \int_0^{x_0^{*(1)}} \sin(m\pi x^*) \sin(n\pi x^*) dx^* \\ & + (n\pi)^2 \sum_{i=1}^{NG-1} T^*(x_e^{*(i)}) \int_{x_e^{*(i)}}^{x_0^{*(i+1)}} \sin(m\pi x^*) \sin(n\pi x^*) dx^* \\ & + (n\pi)^2 T^*(0) \int_{x_e^{*(NG)}}^{1} \sin(m\pi x^*) \sin(n\pi x^*) dx^* \end{aligned} \tag{B4}$$

$$K_{nc}^{(m,n)} = (n\pi) \sum_{i=1}^{NG} \frac{\mu_z^{(i)}}{R^{*(i)}} T^*[x_0^{*(i)}] \int_{x_0^{*(i)}}^{x_e^{*(i)}} \exp\left(\frac{\mu_x^{(i)}(x^* - x_0^{*(i)})}{R^{*(i)}} \right) \times \sin(m\pi x^*) \cos(n\pi x^*) dx^* \tag{B5}$$

References

[1] Hinteregger, H., and Müftü, S., 1996, "Contact Tape Recording With a Flat Head Contour," IEEE Trans. Magn., **32**, pp. 3476–3478.

[2] Wickert, J. A., 1993, "Free Linear Vibration of Self-Pressurized Foil Bearings," ASME J. Vibr. Acoust., **115**, pp. 145–151.

[3] Müftü, S., and Benson, R. C., 1996, "A Study of Cross-Width Variations in the Two-Dimensional Foil Bearing Problem," ASME J. Tribol., **118**, pp. 407–414.

[4] Heinrich, J. C., and Connolly, D., 1992, "Three-Dimensional Finite Element Analysis of Self-Acting Foil Bearings," Comput. Methods Appl. Mech. Eng., **100**, pp. 31–43.

[5] Lakshmikumaran, A. V., and Wickert, J. A., 1999, "Equilibrium Analysis of Finite Width Tension Dominated Foil Bearings," ASME J. Tribol., **121**, pp. 108–113.

[6] Sun, J.-H., and Fung, R.-F., 2003, "A New Dynamic Modelling of the Magnetic Tape Recording System," J. Sound Vib., **259**(3), pp. 637–648.

[7] Zwettler, C. J., Fahimi, S. A., Mewes, M. A., and Johnson, D. W., 2005, "Data Storage Tape Cartridge With Sub-Ambient Pressure Feature," U.S. Patent No. 6,874,720.

[8] Ono, K., 1979, "Lateral Motion of an Axially Moving String on a Cylindrical Guide Surface," ASME J. Appl. Mech., **46**(4), pp. 905–912.

[9] Yang, R. J., 1994, "Steady Motion of a Thread Over a Rotating Roller," ASME J. Appl. Mech., **61**(1), pp. 16–22.

[10] Schajer, G. S., 1984, "The Vibration of a Rotating Circular String Subject to a Fixed Elastic Restraint," J. Sound Vib., **92**(1), pp. 11–19.

[11] Afolabi, D., 1997, "Stability of a Translating Beam With Fixed and Moving Viscous Damping," J. Sound Vib., **199**(4), pp. 701–703.

[12] Garziera, R., and Amabili, M., 2000, "Damping Effect of Winding on the Lateral Vibrations of Axially Moving Tapes," ASME J. Vibr. Acoust., **122**(1), pp. 49–53.

[13] Cheng, S.-P., and Perkins, N. C., 1991, "The Vibration and Stability of a Friction-Guided, Translating String," J. Sound Vib., **144**(2), pp. 281–292.

[14] Zen, G., and Müftü, S., 2006, "Stability of an Axially Accelerating String Subjected to Frictional Guiding Forces," J. Sound Vib., **289**, pp. 551–576.

[15] Chen, J.-S., 1997, "Natural Frequencies and Stability of an Axially-Traveling String in Contact With a Stationary Load System," ASME J. Vibr. Acoust., **119**, pp. 152–157.

[16] Wickert, J. A., and Mote, Jr., C. D., 1990, "Classical Vibration Analysis of Axially-Moving Continua," ASME J. Appl. Mech., **57**(3), pp. 738–744.

[17] Wickert, J. A., and Mote, Jr., C. D., 1991, "Traveling Load Response of an Axially-Moving String," J. Sound Vib., **149**(2), pp. 267–284.

[18] Wickert, J. A., and Mote, Jr., C. D., 1991, "Response and Discretization Methods for Axially-Moving Materials," Appl. Mech. Rev., **44**(11), pp. 279–284.

[19] Kartik, V., and Wickert, J. A., 2006, "Vibration and Guiding of Moving Media With Edge Weave Imperfections," J. Sound Vib., **291**(1–2), pp. 419–436.

[20] Chakraborty, G., and Mallik, A. K., 1999, "Non-Linear Vibration of a Travelling Beam Having an Intermediate Guide," Nonlinear Dyn., **20**(3), pp. 247–265.

[21] Jha, R. K., and Parker, R. G., 2000, "Spatial Discretization of Axially-Moving Media Vibration Problems," ASME J. Vibr. Acoust., **122**, pp. 290–294.

[22] Nayfeh, A. H., and Mook, D. T., 1979, "Nonlinear Oscillations," Wiley, New York, pp. 105–107.